Buck-Boost PFC Converter with Active Power Decoupling Capability Using Time-sharing Control

Yuki Miyada
Dept. of Electrical, Electronics, and Information Engineering
Nagaoka University of Technology
Niigata, Japan
s20318786@stn.nagaokaut.ac.jp

Keita Ohata
Dept. of Science of Technology Innovation
Nagaoka University of Technology
Niigata, Japan
keita_ohata@stn.nagaokaut.ac.jp

Hiroki Watanabe
Dept. of Electrical, Electronics, and Information Engineering
Nagaoka University of Technology
Niigata, Japan
hwatanabe@vos.nagaokaut.ac.jp

Jun-ichi Itoh
Dept. of Science of Technology Innovation
Nagaoka University of Technology
Niigata, Japan
itoh@vos.nagaokaut.ac.jp

***Abstract*—This paper proposes a single-phase buck-boost PFC converter with active power decoupling (APD) using time-sharing control. The features of the proposed circuit are; 1) PFC and APD capability without additional inductors by sharing circuit components and 2) a wide DC voltage control owing to the buck-boost operation. The proposed method is characterized by two operating modes, discontinuous current mode (DCM) and triangular current mode (TCM). At the DCM method, time-sharing control is achieved by operating PFC and APD during each zero current period. In contrast, the TCM method achieves zero-voltage switching when switching between PFC and APD operation. Thus, switching loss is reduced compared to the DCM method. The validity of the proposed circuit operated in DCM is experimentally demonstrated by a 200-W prototype. It was confirmed that the output current ripple at twice the grid frequency is reduced by 90% in the experiment. Furthermore, the operation of the proposed circuit operated in TCM is demonstrated by simulation.**

Keywords— single-phase buck-boost PFC converter, active power decoupling, time-sharing, discontinuous current mode, triangular current mode, zero voltage switching

I. INTRODUCTION

Recently, single-phase AC-DC converters are widely applied in power supplies of home appliances. High harmonics generation and low power factor by the power supplies cause problems in power transmission and distribution systems. In order to solve these problems, a power factor correction (PFC) circuit has been studied and developed[1]-[3]. Several types of PFC circuits have been proposed, such as boost, buck, and buck-boost types. The buck-boost PFC circuits are used in applications requiring a wide DC voltage range. In addition, a bulky electrolytic capacitor is necessary on the DC link to remove the single-phase power ripple. However, the lifetime of an electrolytic capacitor is highly dependent on the environmental temperature [4]. Moreover, the volume of electrolytic capacitors is large, which leads to an increase in the circuit volume.

In contrast, active power decoupling (APD) circuits have been proposed to reduce the size of DC-link capacitors [5]-[19]. The APD circuit uses a small film or ceramic capacitor as a buffer capacitor instead of an electrolytic capacitor. The output instantaneous power fluctuation is compensated by pulsating the power of the buffer capacitor at twice the grid frequency. However, several APD circuits require additional inductors to regulate the buffer capacitor voltage. Therefore, the power density may decrease due to bulky passive components.

This paper proposes single-phase buck-boost PFC converter with APD circuit using time-sharing control. The proposed circuit achieves a wide output voltage range by the four-switch buck-boost PFC converter. The originality of this paper is the time-sharing control strategy for APD, buck and boost in one cycle of switching period. The proposed time-sharing control has no control interference among APD, buck and boost. Furthermore, the number of inductors and switching devices are reduced by sharing circuit components.

In this paper, two types of inductor current control modes are explained to achieve time-sharing control. First, the proposed circuit's operating method in discontinuous current mode (DCM) is discussed. The validity of the proposed circuit operated in DCM is experimentally demonstrated by a 200-W prototype. Next, the method of operating in triangular current mode (TCM) is discussed. The operation of the proposed circuit operated in TCM is demonstrated by simulation.

II. PROPOSED PFC CONVERTER CONFIGURATION

Fig.1 shows the proposed single-phase buck-boost PFC circuit with an APD circuit. The APD circuit consists of only a small buffer capacitor and the switching device of SW_3. The buck-boost PFC converter is used for the PFC capability, DC voltage control, and active power decoupling capability. The AC side leg of the buck-boost PFC circuit is Leg 1 and the DC side leg is Leg 2.

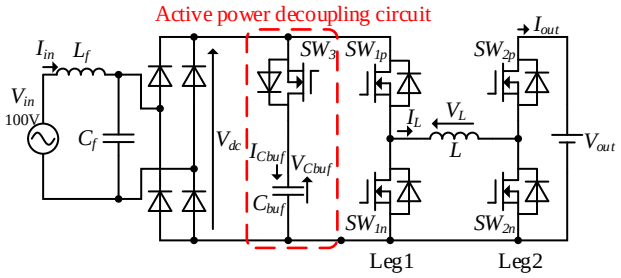

Fig. 1. proposed circuit configuration.

III. Control Method for DCM Operation

The proposed PFC converter has three modes for the V_{out} control depending on the relationship between the diode rectifier output voltage V_{dc} and the output voltage V_{out} as follows;

1. $V_{dc} < V_{out}$: Leg1 driving mode (buck operation)
2. $V_{dc} > V_{out}$: Leg2 driving mode (boost operation)
3. $V_{dc} \approx V_{out}$: 4-arm driving mode

Moreover, the converter has two modes for APD operation:

1. C_{buf} charge mode
2. C_{buf} discharge mode

Fig. 2, Fig. 3 and Fig. 4 show the inductor current waveform and switching pattern for one switching period. In the proposed circuit, PFC and APD operation is achieved within one switching period by using time-sharing control by DCM. Thus, there are six control patterns in one switching period. Fig. 2 shows the waveforms of the Leg1 driving mode, Fig. 3 shows the Leg2 driving mode, and Fig. 4 shows the 4-arm driving mode. The current of C_{buf} flows through the inductor L from the output side by switching SW_{1p} and SW_{1n} during the zero current period of PFC operation.

Generally, a buck-boost operation for PFC is implemented using Leg1 driving and Leg2 driving mode. However, the input current is distorted due to an over-modulation in the condition that V_{dc} and V_{out} are almost same. In order to solve this problem, the 4-arm driving mode is added. In 4-arm driving mode, SW_{1p} and SW_{2n} switches in period T_1, and SW_{1n} and SW_{2p} switches in period T_2. The inductor voltage V_L does not be small in the condition that V_{dc} and V_{out} are almost same, thus over-modulation does not occur in 4-arm driving mode. Hence, the proposed circuit achieves low harmonic distortion current waveforms. During the PFC operation, the APD circuit is disconnected from the PFC circuit by turning SW_3 off, and during the APD operation, SW_3 is turned on to charge and discharge the C_{buf}. The buffer capacitor voltage V_{Cbuf} is controlled to be higher than the peak of input voltage and V_{out}. Thus, the body diode of SW_3 does not conduct.

Fig. 5 shows the input current control block diagram. The duty ratios of periods $T_1 \sim T_4$ in Fig. 2, Fig. 3 and Fig. 4 are defined as $d_1 \sim d_4$. These duties are calculated from the inductor current in DCM condition. The duty ratios in each mode are given by the following equations:

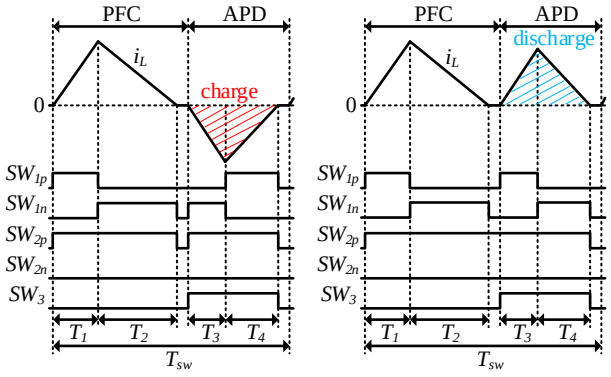

(a) charge mode (b) discharge mode

Fig. 2. Inductor current waveform and switching pattern for one switching period at Leg1 driving mode.

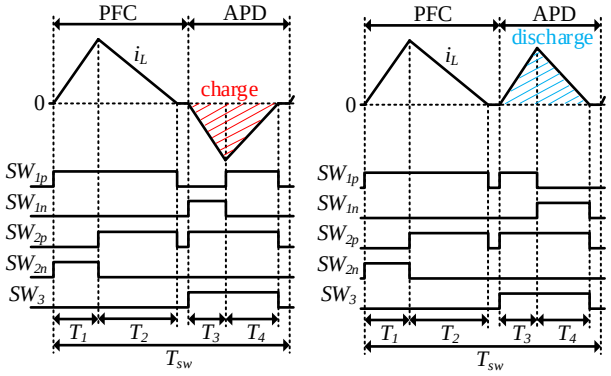

(a) charge mode (b) discharge mode

Fig. 3. Inductor current waveform and switching pattern for one switching period at Leg2 driving mode.

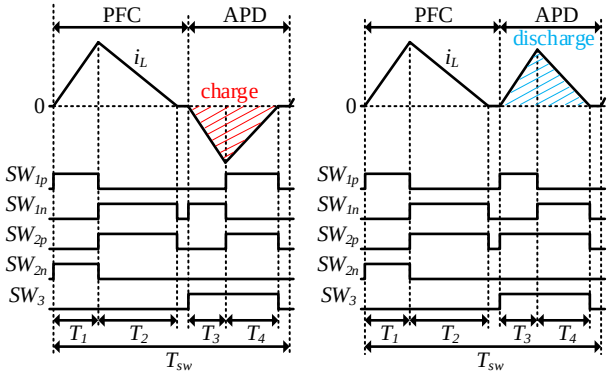

(a) charge mode (b) discharge mode

Fig. 4. Inductor current waveform and switching pattern for one switching period at 4-arm driving mode.

<For Leg1 driving mode>

$$d_{1\_Leg1} = \sqrt{\frac{2L}{(V_{dc} - V_{out})T_{sw}} i_{in}^{*}} \quad \text{.....(1),}$$

$$d_{2\_Leg1} = d_{1\_Leg1} \frac{V_{dc} - V_{out}}{V_{out}} \quad \text{.....(2),}$$

<For Leg2 driving mode>

$$d_{1\_Leg2} = \sqrt{\frac{2L(V_{out} - V_{dc})}{V_{dc} V_{out} T_{sw}} i_{in}^{*}} \quad \text{.....(3)},$$

$$d_{2\_Leg2} = d_{1\_Leg2} \frac{V_{dc}}{V_{out} - V_{dc}} \quad \text{.....(4)},$$

<For 4-arm driving mode>

$$d_{1\_4-arm} = \sqrt{\frac{2L}{V_{dc} T_{sw}} i_{in}^{*}} \quad \text{.....(5)},$$

$$d_{2\_4-arm} = d_{1\_4-arm} \frac{V_{dc} + V_{out}}{V_{out}} \quad \text{.....(6)},$$

where i_{in}^{*} is the input current command, V_{dc} is the diode rectifier output voltage, V_{out} is the output voltage, L is the inductance, and T_{sw} is the switching period. These duties are uniquely determined from (1), (2), (3), (4), (5), and (6). Hence, any feedback control is not needed for input current control.

Fig. 6 shows the control block diagram for buffer capacitor voltage control. The input instantaneous power p_{in} under the unity power factor is given by

$$\begin{aligned} p_{in} &= V_m I_m \sin^2(\omega_{grid} t) \\ &= \frac{V_m I_m}{2}\left\{1 - \cos(2\omega_{grid} t)\right\} \end{aligned} \quad \text{.....(7)},$$

where V_m and I_m are the maximum values of grid voltage and current, and ω_{grid} is the grid angular frequency. The second term in (1) means that the input instantaneous power fluctuates at twice the grid frequency. Thus, the buffer capacitor voltage V_{Cbuf} must be controlled to fluctuate with the frequency of $2\omega_{grid}$. The inductor current command is given by

$$i_{Lbuf}^{*} = \frac{P_n}{V_{out}} \cos(2\omega_{grid} t) \quad \text{.....(8)},$$

where P_n is the input power. A wide bandwidth control in the PI controller for V_{Cbuf} is not required because the average voltage of buffer capacitor V_{Cbuf_ave} and the command value V_{Cbuf}^{*} are not instantaneous values, respectively. Note that the switching between charging and discharging operations is determined by the positive or negative polarity of the inductor current command value i_L^{*}.

IV. Experimental Result at DCM Operation

Table. 1. shows the experimental conditions. The operation of the prototype circuit was tested under the following two voltage and power conditions.

1. Buck-boost operation condition :

   V_{out} = 100 V, P_n = 100 W

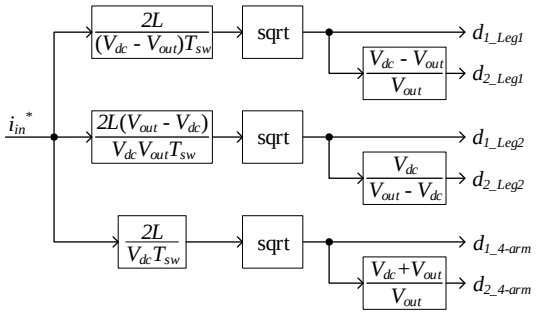

Fig. 5. Proposed input current control block for buck-boost PFC converter.

Table. 1. Experimental parameters at DCM operation

Items	Value
Grid voltage V_{in}	100 V_{rms}
Grid angular frequency ω_{grid}	$2\pi \cdot 50$ rad/s
Inductor L	33 µH
Buffer capacitor C_{buf}	47 µF
Input filter inductor L_f	1.3 mH
Input filter capacitor C_f	1 µF
Switching frequency f_{sw}	50 kHz
Voltage control natural frequency ω_n	100 rad/s
Voltage control damping factor ζ	0.707

2. Boost operation condition : V_{out} = 200 V, P_n = 200 W

Fig. 7 (a) shows the operating waveforms under the buck-boost operation condition (V_{out} = 100V, P_n = 100W). The buffer voltage command V_{Cbuf}^{*} is set to 230V. In the buck-boost operation condition, the operation mode switches between Leg1, Leg2, and 4-arm driving modes within the grid period by the relationship of the voltage amplitude between V_{dc} and V_{out}. The 4-arm driving mode is applied when the condition of $|V_{dc} - V_{out}| < 20$V is satisfied. Fig. 7 (a) shows that the proposed circuit achieves an input current power factor of 0.98 and an input current THD of 5.2%. In addition, the efficiency was 89.5% under the buck-boost operation condition. Fig. 7 (b) shows the operating waveforms under the boost operation condition (V_{out} = 200V, P_n = 200W). Active power decoupling was applied, and the average value of V_{Cbuf} was set to 300V. Fig. 7 (b) shows that the proposed circuit achieves an input current power factor of 0.99 and an input current THD of 5.3%. In addition, the efficiency was 90.2% under the boost operation condition.

Fig. 8 (a) shows the output current harmonics analysis results for the buck-boost operation condition, and Fig. 8 (b) shows the boost operation condition. Fig. 8. shows that the 2nd-order harmonics (100 Hz) of the output current are reduced by more than 90% by applying APD under both conditions.

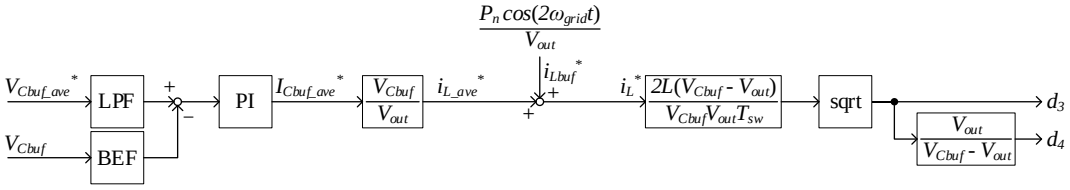

Fig. 6. Proposed buffer capacitor voltage control block diagram for APD circuit.

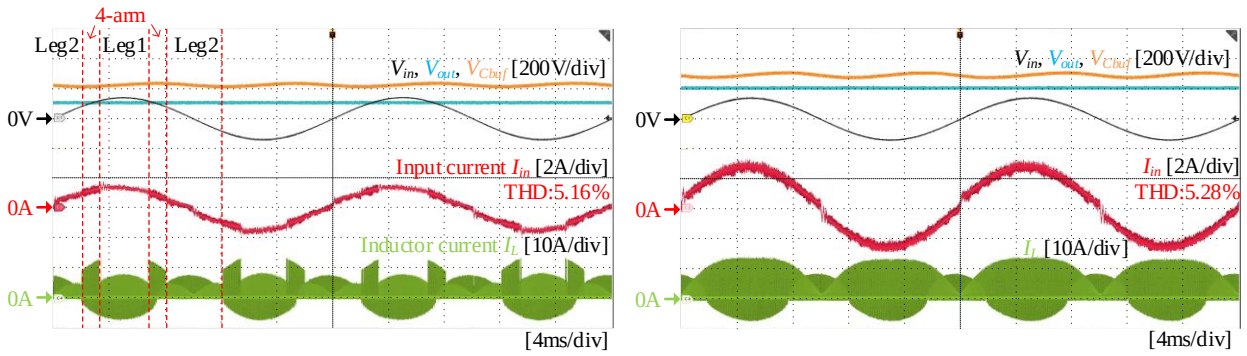

(a) buck-boost operation condition (V_{out} = 100V, P_n = 100W)

(b) Boost operation condition (V_{out} = 200V, P_n =200W)

Fig. 7. Operating waveform when the proposed DCM-based time-sharing control is applied.

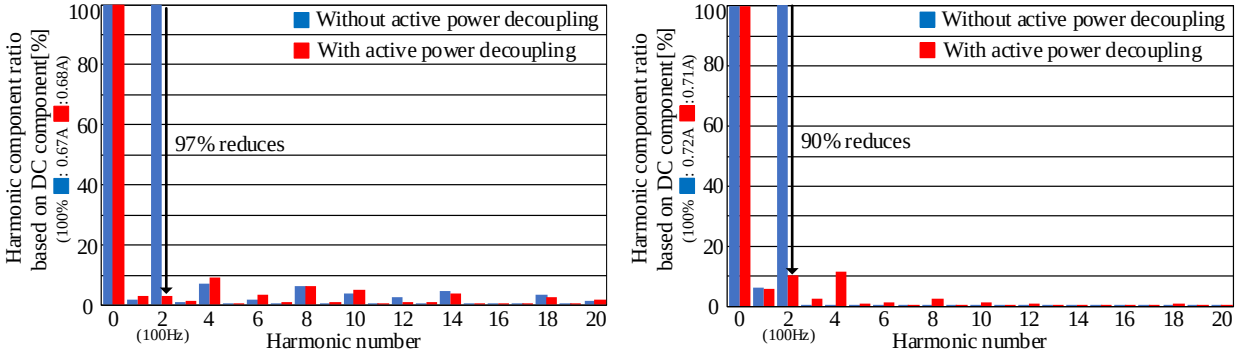

(a) buck-boost operation condition (V_{out} = 100V, P_n = 100W)

(b) Boost operation condition (V_{out} = 200V, P_n =200W)

Fig. 8. Output current harmonics analysis results when the proposed DCM-based time-sharing control is applied.

From the experimental results, the proposed circuit and control method has been achieved for PFC and APD operation. However, the problem of the proposed method is that the maximum efficiency is only 90.2%. One of the reasons for this problem is that zero voltage switching (ZVS) is not achieved at DCM operation when the operation is switched between PFC and APD.

V. Control Method For TCM Operation

In this chapter, the time-sharing control using TCM is explained. This control method extends the time-sharing control using DCM described in the previous chapter. By operated in TCM, it is possible to achieve ZVS[20]-[22] when operation is switched, and high efficiency is achieved through the reduction of switching losses.

Fig. 9, Fig. 10 and Fig. 11 show the inductor current waveform and switching pattern for one switching period at TCM. The PFC operation is applied in the first half of one switching period, and the APD operation is applied in the second half. Depending on the voltage conditions, one of three modes for the PFC operation is selected from Leg1, Leg2, and 4-arm driving modes. In addition, one of two modes for the APD operation from C_{buf} charging and discharging mode. Hence, there are six control patterns in one switching period, the same as in the DCM method. Fig. 9 shows the waveforms of the Leg1 driving mode, Fig. 10 shows the Leg2 driving mode, and Fig. 11 shows the 4-arm driving mode. In the proposed method, TCM operation is achieved by the negative current flow during the switching time from PFC to APD operation (T_2 - T_3 period), as shown in Fig. 9, Fig. 10 and Fig. 11. The inductor current is controlled separately for PFC and APD operation by switching the operation with the set bottom current I_{bot} and top current I_{top}. TCM operation achieves ZVS by the negative current of switching devices during the dead time. Thus, the switching period T_{sw} must be controlled in TCM according to the current command value in order to achieve ZVS. In addition, T_{sw} is related to achieving two current command values, which are PFC and APD operation. Hence, the T_{sw} is determined by three current commands which are for the required negative current of switching devices for ZVS, the PFC current and the APD current.

Fig. 12 shows the control block diagram of the proposed control method. The input current command i_{in}^* is calculated based on the power command value. The APD current command i_{APD}^* is the same as in the DCM method: the charge/discharge current command i_{Lbuf}^*(8) is added to the output of the PI controller that controls the average buffer capacitor voltage V_{Cbuf_ave}. The power pulsation is compensated by pulsating V_{Cbuf} through adding i_{Lbuf}^* to the PI controller output.

The operating time of each switching pattern is expressed as T_1, T_2, T_3 and T_4. The PFC operation period T_1, the APD operation period T_3 and switching period T_{sw} must be calculated from the operating conditions. In contrast, T_2 and T_4 are uniquely determined from the time to reach the bottom current I_{bot} and top current I_{top}, respectively. Thus, the derivation of T_{sw}, T_1, and T_3

is explained using the Leg 1 driving mode and discharge mode. T_{sw} is derived so that the current average current values of PFC and APD operations within one switching period are equal to each current command value. However, deriving T_{sw} requires solving nonlinear simultaneous equations that need to be obtained by numerical analysis. The switching frequency T_{sw} is not uniquely derived from an analytical calculation. Therefore, in this paper, T_{sw} is derived by approximating the equation as $I_{bot} = I_{top} = 0$, which makes the equation analyzable. T_{sw} for Leg 1 drive and discharge mode, which is derived using approximation, is expressed in (9).

$$T_{sw} = \frac{4L}{V_{out}\left(V_{Cbuf} - V_{out}\right)}\left(V_{Cbuf} i^*_{APD} \pm \sqrt{\frac{V_{Cbuf} V_{dc}^2 i^*_{APD} i^*_{in}\left(V_{Cbuf} - V_{out}\right)}{V_{out}\left(V_{dc} - V_{out}\right)}}\right) - \frac{2L\left(V_{dc}^2 V_{out} i^*_{in} - V_{Cbuf} V_{dc}^2 i^*_{in} + V_{Cbuf} V_{dc} V_{out} i^*_{APD} - V_{Cbuf} V_{out}^2 i^*_{APD}\right)}{V_{out}^2\left(V_{Cbuf} - V_{out}\right)\left(V_{dc} - V_{out}\right)} + \left(\frac{V_{Cbuf}}{V_{Cbuf} - V_{out}}\right) 2L i_{bot} \quad \text{.....(9).}$$

The command values for periods T_1 and T_3 are derived based on (9). The period T_1 is derived from the input current command and the period T_3 is derived from the APD current command value using (10) and (11).

$$T_1 = \sqrt{\frac{2LT_{sw}}{V_{dc} - V_{out}} i_{ave\_PFC}} + \frac{L}{V_{Cbuf} - V_{out}} i_{bot} \quad \text{.....(10)}$$

$$T_3 = \sqrt{\frac{2LV_{out}T_{sw}}{V_{Cbuf}\left(V_{Cbuf} - V_{out}\right)} i_{ave\_APD} + \frac{2L^2 i_{bot}^2}{\left(V_{Cbuf} - V_{out}\right)^2}} + \frac{L}{V_{Cbuf} - V_{out}} i_{bot} \quad \text{.....(11)}$$

Note that the results of deriving T_{sw}, T_1, and T_3 for the other operating modes are shown in the Appendix.

VI. Simulation Result at TCM Operation

The proposed control method is verified by simulation under two voltage and power conditions similar to the experimental conditions at DCM operation. Table. 2. shows the simulation conditions. The bottom current I_{bot} and top current I_{top} were set to 0.5 A for both conditions. The output current I_{out_LPF} is the waveform passed through an LPF for observation with a 1 kHz cutoff frequency.

Fig. 13 (a) shows the operating waveforms under the buck-boost operation condition (V_{out} = 100V, P_n = 100W). The output current I_{out_LPF} is the waveform passed through an LPF for observation with a 1 kHz cutoff frequency. The active power decoupling was applied, and the average value of V_{Cbuf} was set to 230V. In the buck-boost operation condition, the operation mode switches between Leg1, Leg2, and 4-arm driving modes within the grid period by the relationship of the voltage amplitude between V_{dc} and V_{out}. Fig. 13 (a) shows that the proposed circuit achieves an input current power factor of 0.99 and an input current THD of 3.2%. Fig. 9 (b) shows the operating waveforms under the boost operation condition (V_{out} = 200V, P_n = 200W). The active power decoupling was applied, and the average value of V_{Cbuf} was set to 300V. Fig. 13 (b) shows that the proposed circuit achieves an input current power factor of 0.98 and an input current THD of 4.7%.

Fig. 14 shows the results of the harmonic analysis of the

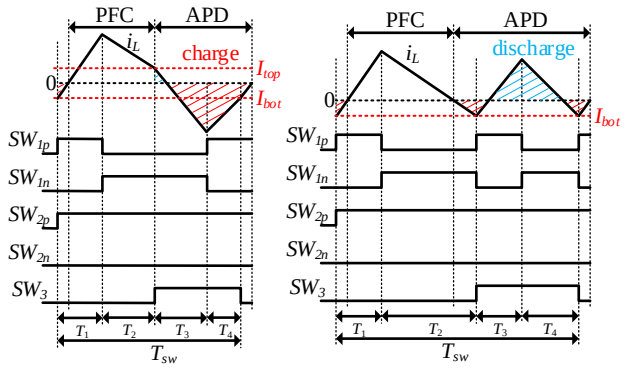

(a) charge mode (b) discharge mode

Fig. 9. Inductor current waveform and switching pattern for one switching period at Leg1 driving mode

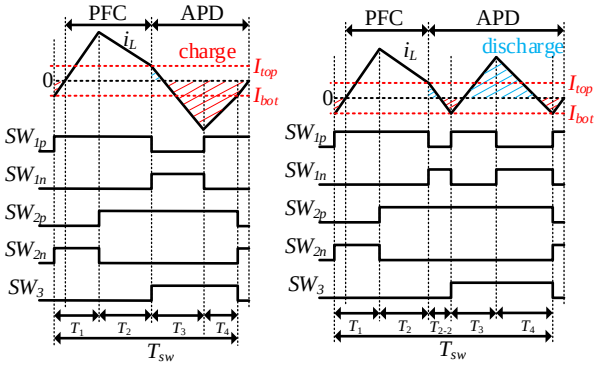

(a) charge mode (b) discharge mode

Fig. 10. Inductor current waveform and switching pattern for one switching period at Leg2 driving mode

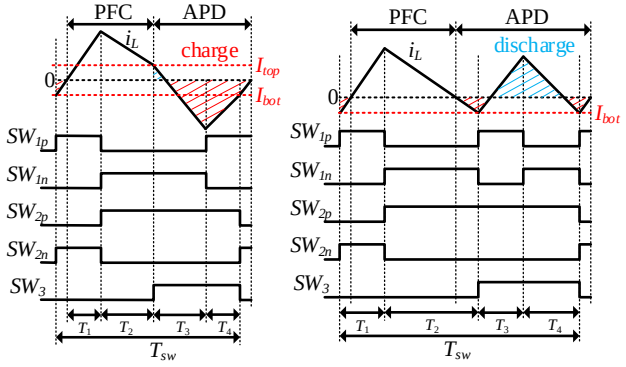

(a) charge mode (b) discharge mode

Fig. 11. Inductor current waveform and switching pattern for one switching period at 4-arm driving mode

output current. Fig. 14 shows that the 2nd-order harmonics (100 Hz) of the output current are reduced by more than 95% in both conditions compared to without APD.

VII. Conclusion

This paper proposed a single-phase buck-boost PFC converter with active power decoupling using the time-sharing control. The proposed circuit achieves a wide output voltage range. In addition, the time-sharing control achieves high power density by sharing the inductor and the devices between PFC and APD operation. The time-sharing control using two types of inductor current modes, DCM and TCM, are proposed. The DCM method was tested under two conditions: buck-boost and boost operation conditions. From the experimental results, it was verified that the input current THD was 5.3% and the power factor was 0.98 under both conditions. In addition, the 2nd-order harmonics (100 Hz) of the output current was reduced by 90%. However, the DCM method has the problem that its maximum efficiency is only about 90%. In contrast, the TCM method reduces switching loss compared to the DCM method by ZVS. The simulation results of the TCM method showed that the proposed control method achieves fundamental PFC and APD operation.

In future works, the efficiency of the TCM method will be compared with that of the DCM method based on the experimental results.

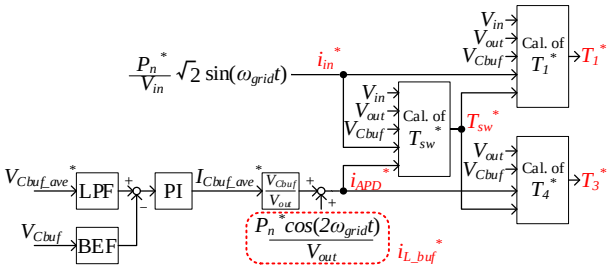

Fig. 12. Control block diagram at TCM operation.

Table 2. Experimental parameters at TCM operation

Items	Value
Grid voltage V_{in}	100 V_{rms}
Grid angular frequency ω_{grid}	$2\pi \cdot 50$ rad/s
Inductor L	250 μH
Buffer capacitor C_{buf}	47 μF
Input filter inductor L_f	1.3 mH
Input filter capacitor C_f	5 μF
Voltage control natural frequency ω_n	100 rad/s
Voltage control damping factor ζ	0.707

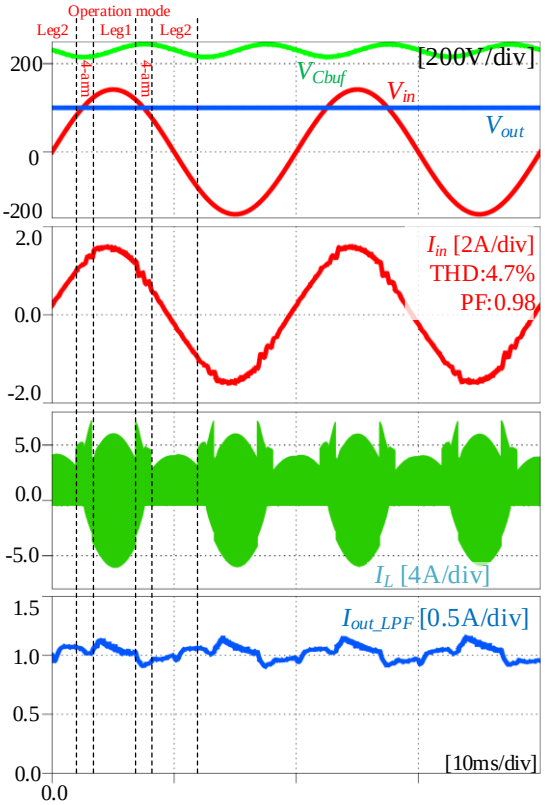

(a) buck-boost operation condition
(V_{out} = 100V, P_n = 100W)

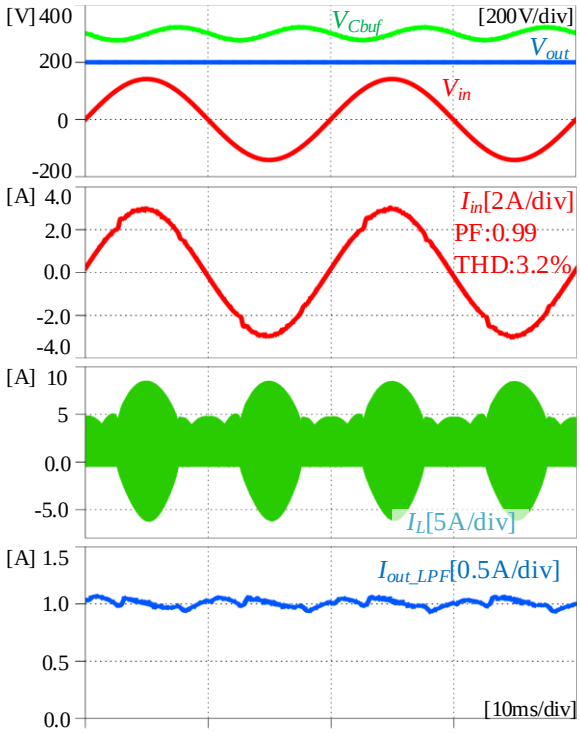

(b) boost operation condition
(V_{out} = 200V, P_n =200W)

Fig. 13. Simulation results when the proposed TCM-based time-sharing control is applied.

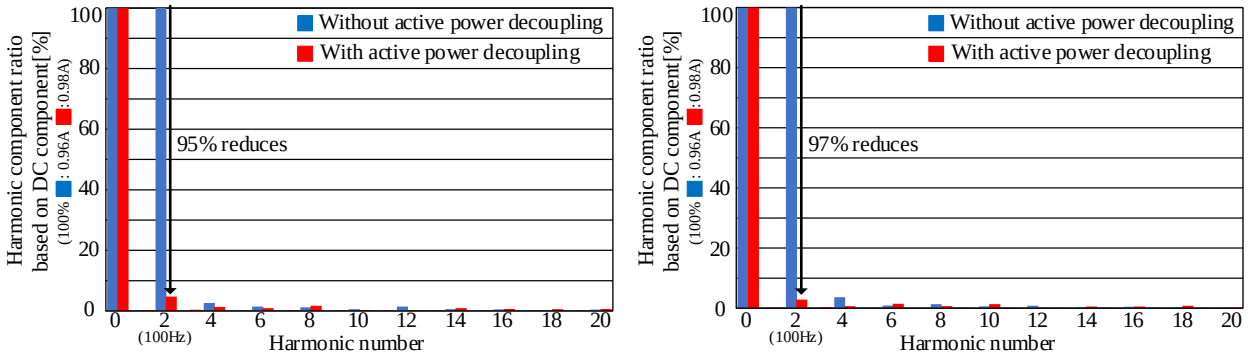

(a) buck-boost operation condition (V_{out} = 100V, P_n = 100W)

(b) boost operation condition (V_{out} = 200V, P_n =200W)

Fig. 14. Output current harmonics analysis results when the proposed TCM-based time-sharing control is applied.

APPENDIX

T_{sw}, T_1, and T_3 in Leg 1 driving and charge mode are derived as follows ;

$$T_1 = \sqrt{\frac{2LT_{sw}}{V_{in}-V_{out}} i_{ave\_PFC}} + \frac{L}{V_{Cbuf}-V_{out}} i_{bot} \quad \text{..... (A-1)}$$

$$T_3 = \sqrt{\frac{2L\left(V_{Cbuf}-V_{out}\right)T_{sw}}{V_{out}V_{Cbuf}}\left|i_{ave\_APD}\right| + \frac{L^2 i_{top}^2}{V_{out}^2 V_{Cbuf}}} + \frac{L}{V_{out}} i_{top} \quad \text{..... (A-2)}$$

$$T_{sw} = \frac{4L}{V_{out}\left(V_{Cbuf}-V_{out}\right)}\left(V_{Cbuf}\left|i_{ave\_APD}\right| + \sqrt{\frac{V_{Cbuf}V_{in}^2(V_{Cbuf}-V_{out})i_{ave\_PFC}\left|i_{ave\_APD}\right|}{V_{out}(V_{in}-V_{out})}}\right)$$
$$+ \frac{2L\left(-V_{in}^2 V_{out} i_{ave\_PFC} + V_{Cbuf}V_{in}^2 i_{ave\_PFC} - V_{Cbuf}V_{in}V_{out}\left|i_{ave\_APD}\right| + V_{Cbuf}V_{out}^2\left|i_{ave\_APD}\right|\right)}{V_{out}^2\left(V_{Cbuf}-V_{out}\right)(V_{in}-V_{out})}$$
..... (A-3)

T_{sw}, T_1, and T_3 in Leg 2 driving and discharge mode are derived as follows ;

$$T_1 = \sqrt{\frac{2L(V_{out}-V_{in})i_{PFC}^* T_{sw} - L^2 i_{top}^2}{V_{in}V_{out}}} + \frac{L}{V_{Cbuf}} i_{bot} \quad \text{..... (A-4)}$$

$$T_3 = \sqrt{\frac{2LV_{out}T_{sw}}{V_{Cbuf}\left(V_{Cbuf}-V_{out}\right)} i_{APD}^* + \frac{L^2 i_{bot}^2\left(V_{Cbuf}^2 + V_{out}V_{Cbuf} - V_{out}^2\right)}{V_{Cbuf}^2\left(V_{Cbuf}-V_{out}\right)^2}}$$
$$+ \frac{L}{V_{Cbuf}-V_{out}} i_{bot}$$
..... (A-5)

$$T_{sw} = \frac{4L}{V_{in}(V_{out}-V_{in})}\left\{V_{out} i_{ave\_PFC} + \sqrt{\frac{V_{Cbuf}V_{in} i_{ave\_APD} i_{ave\_PFC}(V_{out}-V_{in})}{V_{Cbuf}-V_{out}}}\right\}$$
$$+ \frac{2L\left(V_{Cbuf}V_{in}^2 i_{ave\_APD} - V_{Cbuf}V_{in}V_{out} i_{ave\_APD} - V_{out}^3 i_{ave\_PFC} + V_{Cbuf}V_{out}^2 i_{ave\_PFC}\right)}{V_{in}V_{out}\left(V_{Cbuf}-V_{out}\right)(V_{in}-V_{out})}$$
..... (A-6)

T_{sw}, T_1, and T_3 in Leg 2 driving and charge mode are derived as follows ;

$$T_1 = \sqrt{\frac{2L(V_{out}-V_{in})T_{sw}}{V_{in}V_{out}} i_{PFC}^* + \frac{L^2 i_{top}^2}{V_{in}V_{out}}} + \frac{L}{V_{Cbuf}} i_{bot} \quad \text{..... (A-7)}$$

$$T_3 = \sqrt{\frac{2L\left(V_{Cbuf}-V_{out}\right)T_{sw}}{V_{out}V_{Cbuf}}\left|i_{APD}^*\right| + \frac{L^2 i_{bot}^2}{V_{out}V_{Cbuf}} + \frac{L^2\left(V_{Cbuf}-V_{out}\right)\left(V_{Cbuf}i_{bot}^2 - V_{out}i_{top}^2\right)}{V_{out}^2 V_{Cbuf}^2}}$$
$$+ \frac{L}{V_{out}} i_{top}$$
..... (A-8)

$$T_{sw} = \frac{4L}{V_{out}\left(V_{Cbuf}-V_{out}\right)}\left(V_{Cbuf}\left|i_{ave\_APD}\right| + \sqrt{\frac{V_{out}^2 V_{Cbuf}(V_{Cbuf}-V_{out})i_{ave\_PFC}\left|i_{ave\_APD}\right|}{V_{in}(V_{out}-V_{in})}}\right)$$
$$+ \frac{2L\left(-V_{Cbuf}V_{in}^2\left|i_{ave\_APD}\right| + V_{Cbuf}V_{in}V_{out}\left|i_{ave\_APD}\right| + V_{out}^3 i_{ave\_PFC} - V_{Cbuf}V_{out}^2 i_{ave\_PFC}\right)}{V_{in}V_{out}\left(V_{Cbuf}-V_{out}\right)(V_{in}-V_{out})}$$
..... (A-9)

T_{sw}, T_1, and T_3 in 4-arm driving and discharge mode are derived as follows ;

$$T_1 = \sqrt{\frac{2LT_{sw}}{V_{in}} i_{PFC}^*} + \frac{L}{V_{Cbuf}} i_{bot} \quad \text{..... (A-10)}$$

$$T_3 = \sqrt{\frac{2LV_{out}T_{sw}}{V_{Cbuf}\left(V_{Cbuf}-V_{out}\right)} i_{APD}^* + \frac{L^2 i_{bot}^2\left(2V_{Cbuf}^2 - V_{out}^2\right)}{V_{Cbuf}^2\left(V_{Cbuf}-V_{out}\right)^2}}$$
$$+ \frac{L}{V_{Cbuf}-V_{out}} i_{bot}$$
..... (A-11)

$$T_{sw} = \frac{4L}{V_{out}\left(V_{Cbuf}-V_{out}\right)}\left(V_{Cbuf} i_{ave\_APD} + \left(V_{in}+V_{out}\right)\sqrt{\frac{V_{Cbuf} i_{ave\_APD} i_{ave\_PFC}\left(V_{Cbuf}-V_{out}\right)}{V_{in}V_{out}}}\right)$$
$$- \frac{2L(V_{out}^3 i_{ave\_PFC} - V_{in}^2 V_{Cbuf} i_{ave\_PFC} - V_{out}^2 V_{Cbuf} i_{ave\_PFC} + V_{in}V_{out}^2 i_{ave\_PFC}}{V_{in}V_{out}^2\left(V_{Cbuf}-V_{out}\right)}$$
$$\underline{+V_{in}^2 V_{out} i_{ave\_PFC} + V_{Cbuf}V_{in}V_{out} i_{ave\_APD} - 2V_{Cbuf}V_{in}V_{out} i_{ave\_PFC})}$$
..... (A-12)

T_{sw}, T_1, and T_3 in 4-arm driving and charge mode are derived as follows ;

$$T_1 = \sqrt{\frac{2LT_{sw}}{V_{in}} i_{PFC}^*} + \frac{L}{V_{Cbuf}} i_{bot} \quad \text{..... (A-13)}$$

$$T_3 = \sqrt{\frac{2L\left(V_{Cbuf} - V_{out}\right)T_{sw}}{V_{out}V_{Cbuf}}\left|i_{APD}^{*}\right| + \frac{L^2 i_{bot}^2}{V_{out}V_{Cbuf}} - \frac{L^2 i_{bot}^2\left(V_{Cbuf} - V_{out}\right)}{V_{out}V_{Cbuf}^2} + \frac{L^2 i_{top}^2\left(V_{Cbuf} - V_{out}\right)}{V_{out}^2 V_{Cbuf}}} + \frac{L}{V_{out}} i_{top}$$

..... (A-14)

$$T_{sw} = \frac{4L}{V_{out}\left(V_{Cbuf} - V_{out}\right)}\left\{V_{Cbuf}\left|i_{ave\_APD}\right| + \left(V_{in} + V_{out}\right)\sqrt{\frac{V_{Cbuf}\left(V_{Cbuf} - V_{out}\right)i_{ave\_PFC}\left|i_{ave\_APD}\right|}{V_{in}V_{out}}}\right\}$$
$$- \frac{2L(V_{out}^3 i_{ave\_PFC} - V_{Cbuf}V_{in}^2 i_{ave\_PFC} - V_{Cbuf}V_{out}^2 i_{ave\_PFC} + 2V_{in}V_{out}^2 i_{ave\_PFC} + V_{in}^2 V_{out} i_{ave\_PFC}}{V_{in}V_{out}^2\left(V_{Cbuf} - V_{out}\right)}$$
$$\frac{-2V_{Cbuf}V_{in}V_{out}i_{ave\_PFC} + V_{Cbuf}V_{in}V_{out}\left|i_{ave\_APD}\right|)}{}$$

..... (A-15)

REFERENCES

[1] Z. Bing, M. Chen, S. Miller, Y. Nishida, and J. Sun, "Recent developments in single-phase power factor correction," inProc.Power Conversion Conference-Nagoya, 2007. PCC'07, 2007, pp.1520–1526.

[2] L. Huber, L. Gang, and M. M. Jovanovic, "Design-oriented analysisand performance evaluation of buck PFC front end,"IEEE Trans.Power Electron., vol. 25, no. 1, pp. 85–94, 2010.

[3] G. Andersen, "Current programmed control of a single-phase two-switch buck-boost power factor correction circuit,"IEEE Trans. Ind.Elec., vol. 53, no. 1, pp. 263–271, 2006.

[4] H. Hu, S. Harb, X. Fang, D. Zhang, Q. Zhang, Z. J. haen: "A Three-port Fly back for PV Micro inverter Applications With Power Pulsation Decoupling Capability", IEEE Trans., Vol. 27 No. 9, pp. 3953-3964 (2012)

[5] D. Neumayr, G. C. Knabben, E. Varescon, D. Bortis and J. W. Kolar, "Comparative Evaluation of a Full- and Partial-Power Processing Active Power Buffer for Ultracompact Single-Phase DC/AC Converter Systems", IEEE Journal of Emerging and Selected Topics in Power Electronics, Vol. 9, No. 2, pp. 1994-2013, 2021.

[6] Y. Cui, H. Han, Y. Liu, G. Xu, M. Su, and S. Xie, "An Efficiency-Improved Single-Phase PFC Rectifier With Active Power Decoupling", IEEE Transactions on Power Electronics, Vol. 37, No. 9, pp. 10784-10796, September, 2022.

[7] C. B. Barth, I. Moon, Y. Lei, S. Qin, R. C. N. Pilawa-Podgurski: "Experimental Evaluation of Capacitors for Power Buffering in SinglePhase Power Converters", ECCE 2015, pp. 6269-6276 (2015)

[8] S. Yamaguchi, T. Shimizu : "Single-phase Power Conditioner with a Buck-boost-type Power Decoupling Circuit", IEEJ Journal of Industry Applications, Vol. 5, No. 3, pp. 191-198 (2016)

[9] Montie. A, Luciano. F.S Alves, Ruxi. Wang, and Mauricio. B.R. Correa, "Low-Frequency Power Decoupling in Single-Phase Applications overview,"IEEE Transactions on Power Electronics, vol: pp. (2016)

[10] Y. Tang, F. Blaabjerg, "An efficiency improved active power decoupling circuit with minimized implementation cost" 2014 international power electronics and application conference and exposition. pp. 864-869 (2014)

[11] S. Kjaer and J. Pedersen, "A review of single-phase grid-connected inverters for photo-voltaic modules," IEEE Trans. Ind. Ap., vol. 41, no. 5, pp. 1292-1306, (2005)

[12] S. Ma, H. Wang, H. Tang, G. Zhu and H. Wang "Lifetime estimation of DC-link capacitors in a single-phase converter with an integrated active power decoupling module" IECON 2016, pp. 6824-6829 (2016)

[13] V.V.S. Pradeeo Kumar, B.G. Fenabdes "transformerless active power decoupling topologies for grid connected PV applications" IECON 2016, pp. 2410-2419 (2016)

[14] I. Serban, C. Marinescu, D. Munteanu "Performance analysis of a SiC-based single-phase H-bridge inverter with active power decoupling" EPE 2016 pp.1-10 (2016)

[15] S. Qin, Y. Lei, C. Barth, W. -C. Liu and R. C. N. Pilawa-Podgurski, "A high-efficiency high energy density buffer architecture for power pulsation decoupling in grid-interfaced converters," 2015 IEEE Energy Conversion Congress and Exposition (ECCE), pp. 149-157, 2015.

[16] Y. Sun, Y. Liu, X. Li, J. Yang "Active power decoupling method for single-phase current source rectifier with no additional active switches" IEEE trans. vol. 31, pp.5644-5654 (2016)

[17] N. Pragallapati, V. Agarwal, "Single phase solar PV module integrated flyback based micro-inverter with novel active power decoupling" PEMD 2014. pp. (2014)

[18] W. Qi, H. Wang, X. Tan, G. Wang, K. D.T Ngo, "A novel active power decoupling single-phase PWM rectifier topology" APEC 2014. pp. 89-95 (2014)

[19] T. Hirao, T. Shimizu, M. Ishikawa, K. Yasui "Discussion on Modulation Methods for Flyback-type Single-phase Inverters with Enhanced Power Decoupling for Photovoltaic AC module Systems" IEEJ trans., No.4, pp. 504-510 (2006)

[20] J. Zhang, J-S. Lai, R-Y. Kim, W. Yu, "High-Power Density Design of a Soft-Switching High-Power Bidirectional dc–dc Converter", IEEE Transaction on Power Electronics, Vol. 22, No. 4, pp. 1145 - 1153 (2007).

[21] C. Marxgut, F. Krismer, D. Bortis, J. W. Kolar, "Ultraflat Interleaved Triangular Current Mode (TCM) SinglePhase PFC Rectifier", IEEE Transaction on Power Electronics, Vol. 29, No. 2, pp. 873 - 882 (2014).

[22] X. Huang, F. C. Lee, Q. Li, W. Du, "HighFrequency High-Efficiency GaN-Based Interleaved CRM Bidirectional Buck/Boost Converter with Inverse Coupled Inductor", IEEE Transaction on Power Electronics, Vol. 31, No. 6, pp. 4343 - 4352 (2015).